ACS APPLIED MATERIALS & INTERFACES

Research Article

www.acsami.org

Tunable Luminescent Properties and Concentration-Dependent, Site-Preferable Distribution of Eu^{2+} Ions in Silicate Glass for White LEDs Applications

Xuejie Zhang,[†] Jing Wang,*[,†] Lin Huang,[†] Fengjuan Pan,[†] Yan Chen,[‡] Bingfu Lei,[§] Mingying Peng,[⊥] and Mingmei Wu*[,†]

[†]Ministry of Education Key Laboratory of Bioinorganic and Synthetic Chemistry, State Key Laboratory of Optoelectronic Materials and Technologies, KLGHEI of Environment and Energy Chemistry, School of Chemistry and Chemical Engineering, and [‡]School of Physics and Engineering, Sun Yat-sen University, Guangzhou, Guangdong 510275, China

[§]Department of Applied Chemistry, South China Agriculture University, Guangzhou, Guangdong 510642, China

[⊥]School of Materials Science and Technology, South China University of Technology, Guangzhou 510640, China

Supporting Information

ABSTRACT: The design of luminescent materials with widely and continuously tunable excitation and emission is still a challenge in the field of advanced optical applications. In this paper, we reported a Eu^{2+}-doped SiO_2-Li_2O-SrO-Al_2O_3-K_2O-P_2O_5 (abbreviated as SLSAKP:Eu^{2+}) silicate luminescent glass. Interestingly, it can give an intense tunable emission from cyan (474 nm) to yellowish-green (538 nm) simply by changing excitation wavelength and adjusting the concentration of Eu^{2+} ions. The absorption spectra, photoluminescence excitation (PLE) and emission (PL) spectra, and decay curves reveal that there are rich and distinguishable local cation sites in SLSAKP glasses and that Eu^{2+} ions show preferable site distribution at different concentrations, which offer the possibility to engineer the local site environment available for Eu^{2+} ions. Luminescent glasses based color and white LED devices were successfully fabricated by combining the as-synthesized glass and a 385 nm n-UV LED or 450 nm blue LED chip, which demonstrates the potential application of the site engineering of luminescent glasses in advanced solid-state lighting in the future.

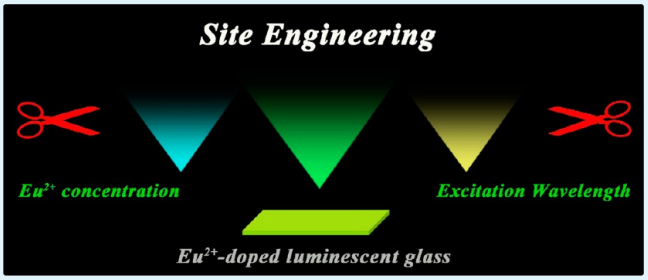

KEYWORDS: *tunable light, silicate glass, Eu^{2+} ion, sites, LED device*

1. INTRODUCTION

Luminescent materials with widely and continuously tunable excitation and emission have been intensely researched in recent years because of their manifold range of potential application, such as color display technologies, high-efficiency solid-state lighting, information storage, biological sensing and labeling, as well as photoelectronic and photonic devices.[1−8]

Generally, there are three approaches to designing luminescent crystalline materials with tunable emitting light. First, one can select different activator or sensitizer/activator pairs in the same host to develop tunable emitting phosphors. For instance, Y_2O_2S:Eu^{3+} and Y_2O_2S:Tb^{3+} are commercial red and green emitting phosphors for traditional color CRT, respectively,[9,10] and $Ca_5(PO_4)_3(Cl,F)$:Sb^{3+}/Mn^{2+} is commercially tunable blue-to-yellow as well as white emitting phosphor activated by donor (Sb^{3+})-acceptor (Mn^{2+}) pairs for fluorescent lamp in the field of traditional lighting.[11,12] Second, tunable emitting phosphors can be designed by modifying the host composition doping with the specific activator. For example, Eu^{2+} ion can emit intense blue, green, and red emission in $BaMgAl_{10}O_{17}$ (BAM), β-SiAlON, and $Sr_2Si_5N_8$, respectively, which are all commercial phosphors for white light-emitting diodes (white LEDs) in the field of solid-state lighting.[13−21] Unfortunately, tunable excitation and emission cannot be realized in those phosphors mentioned above once the host/activator composition and the concentration of activator are fixed.

In addition to the two methods mentioned above, the well-known crystallographic site engineering has also provided a useful tool for producing phosphors with tunable excitation and emission.[22−25] For examples, Yasushi Sato et al. reported that Eu^{2+} ions occupy two different crystallographic Ca sites in Ca_2SiO_4 and give tunable emission from green-yellow to deep-red with increasing Eu^{2+} concentration.[22] Unfortunately, the phosphor does not exhibit tunable emissions at fixed concentration of Eu^{2+} ions. Jia Zhang et al. reported that at fixed Eu^{2+} concentration, Eu^{2+} ions occupy three different crystallographic Ca sites in $Ca_{14}Mg_2(SiO_4)_8$ and give tunable

Received: March 23, 2015
Accepted: April 21, 2015
Published: April 21, 2015

DOI: 10.1021/acsami.5b02550
ACS Appl. Mater. Interfaces 2015, 7, 10044−10054

green emissions from 504 to 508 nm under excitation of 296, 330, and 396 nm.[24] Unfortunately, the emission of Eu^{2+} is limited in tunable range. In summary, a limited number of cation sites with distinguishable crystalline environment or a number of cation sites with similar crystalline environment in a specific host compound will poorly contribute to tunable excitation and emission. Comparatively, glasses are a vital class of noncrystalline materials and have the merit of short-range order and long-range disorder,[26,27] which possess abundant and continuously distinguishable sites available for luminescent activators. Consequently, this theoretically makes it easier to use site engineering to design tunable excitation and emission in glasses, which may be wider and more continuous than that in crystalline compounds. In 2012, L. H. C. Andrade et al.[28] reported Ce^{3+}-doped low-silica-calcium-alumino-silicate glass, of which the emission color can be widely tuned from blue to yellow under different excitation wavelengths. Thereafter, they reported Eu^{2+}-doped calcium aluminosilicate glass,[29] which also gives the tunable emission from green to orange by using different excitation wavelengths and varying concentration of Eu^{2+} ions. Unfortunately, the underlying luminescent mechanisms in rare earth ion-doped glass are still unclear, which hinders the improvement on the performance of luminescent glasses with widely and continuously tunable excitation and emission in the future. In this paper, we reported Eu^{2+} ion-doped silicate glasses and systematically studied the relationship between the sites and tunable PLE and PL through absorption spectra, steady-state PLE and PL spectra, and decay curves. Moreover, we demonstrated their potential applications in color and white LED devices.

2. EXPERIMENTAL SECTION

2.1. Sample Preparation. Both the mother glass and Eu^{2+}-doped glasses were prepared by the conventional melt-quenching method. The precursor glass has the composition (mol %) of $45SiO_2$-$30Li_2O$-$15SrO$-$5Al_2O_3$-$3K_2O$-$2P_2O_5$ and the Eu^{2+}-doped SLSAKP glasses are referred to as SLSAKP:xEu^{2+}, where x = 0.05, 0.10, 0.20, 0.40, 0.80, and 1.00% (mol %). The analytical pure reagents of the oxides SiO_2 and Al_2O_3, the carbonates Li_2CO_3, $SrCO_3$, and K_2CO_3, the phosphate $NH_4H_2PO_4$, and high pure Eu_2O_3 (4N) were used as raw materials. In a typical melting quenching process, the corresponding raw materials were mixed thoroughly in an agate mortar and the mixtures were then melted in a corundum crucible at 1500 °C for 1 h under thermal-carbon reducing atmosphere. The melts were cast into preheated (500 °C) graphite molds, subsequently annealed for 2 h at 500 °C to relieve the stress, and finally cooled to room temperature. The as-synthesized glasses were cut and carefully polished into specimens of ∼3 mm thickness for optical measurements. The n-UV Chip-On-Board (n-UV COB) and blue chip-on-board (blue COB) LED modules consisted of a 6 × 8 array of n-UV (∼385 nm) chips and 3 × 3 array of blue (∼450 nm) chips, respectively. To obtain the white LEDs, we prepared the $CaAlSiN_3$:Eu^{2+}-based glass plate by Phosphor-in-Glass (PiG) technology.[30,31,51] PiG is a novel composite material that a certain amount of phosphor disperse in an inorganic glass matrix, which is prepared simply by cosintering of the mixture of phosphor and glass powder at low processing temperature. The glass frit was prepared from SiO_2–Al_2O_3–B_2O_3–ZnO–BaO via a conventional melt-quenching method and the commercial red phosphor $CaAlSiN_3$:Eu^{2+} was purchased from LUMING Technology Group Co. Ltd. As a proof-of-concept experiment, the green-emitting luminescent glass based LED (LG-LED) device was fabricated simply by placing a luminescent glass on n-UV COB excitation source. White LED device was constructed simply by first placing SLSAKP:1.00% Eu^{2+} glass on the blue COB chip and then stacking the $CaAlSiN_3$:Eu^{2+}-based PiG on the SLSAKP:1.00% Eu^{2+} glass.

2.2. Characterization. Absorption spectra were recorded with a Cary 5000 UV–vis–NIR spectrophotometer (Varian Instruments) equipped with double out-of-plane Littrow monochromator. The PLE and PL spectra within the temperature range 296–498 K as well as the decay curves were measured using a FSP920 Time Resolved and Steady State Fluorescence Spectrometers (Edinburgh Instruments) equipped with a 450 W Xe lamp, a 150 W nF900 flash lamp, TM300 excitation monochromator and double TM300 emission monochromators and thermo-electric cooled red-sensitive PMT. The spectral resolution for the steady measurements is about 0.05 nm in UV–vis. For PL measurements at above room temperature, the sample was mounted in an Oxford OptistatDN2 nitrogen cryostat. The room temperature internal quantum efficiency (IQE) of sample was measured using a barium sulfate coated integrating sphere attached to the FSP920. QE65000 (Ocean Optics Instruments) was employed to measure the electroluminescence (EL) spectra at a forward current.

3. RESULTS AND DISCUSSION

3.1. Spectroscopic Properties of SLSAKP:Eu^{2+} Glasses. Figure 1a shows the optical absorption spectra of the SLSAKP:xEu^{2+} glasses (x = 0, 0.05, 0.10, 0.20, 0.40, 0.80, and

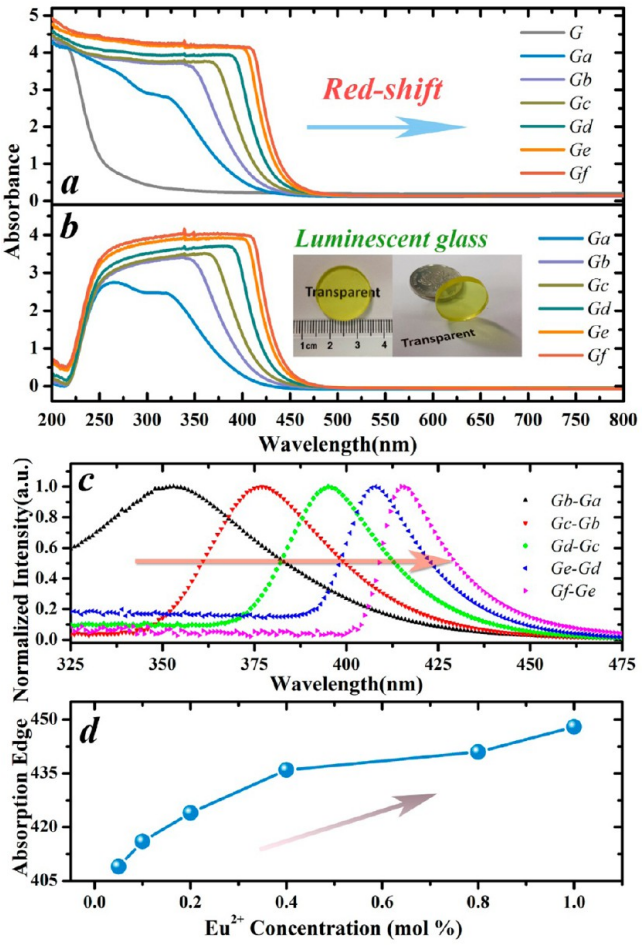

Figure 1. (a) Optical absorption spectra of SLSAKP (G) and SLSAKP:xEu^{2+} (x = 0.05, 0.10, 0.20, 0.40, 0.80, and 1.00% for Ga, Gb, Gc, Gd, Ge, and Gf, respectively) glasses; (b) optical absorption spectra of the as-fabricated glasses obtained by subtracting mother glass SLSAKP from original SLSAKP:xEu^{2+} glass; (c) normalized difference spectra by subtracting the optical spectra of two SLSAKP:Eu^{2+} glasses with adjacent concentrations of Eu^{2+} ions; (d) concentration dependence of long-wavelength absorption edge of Eu^{2+} ions.

DOI: 10.1021/acsami.5b02550
ACS Appl. Mater. Interfaces 2015, 7, 10044–10054

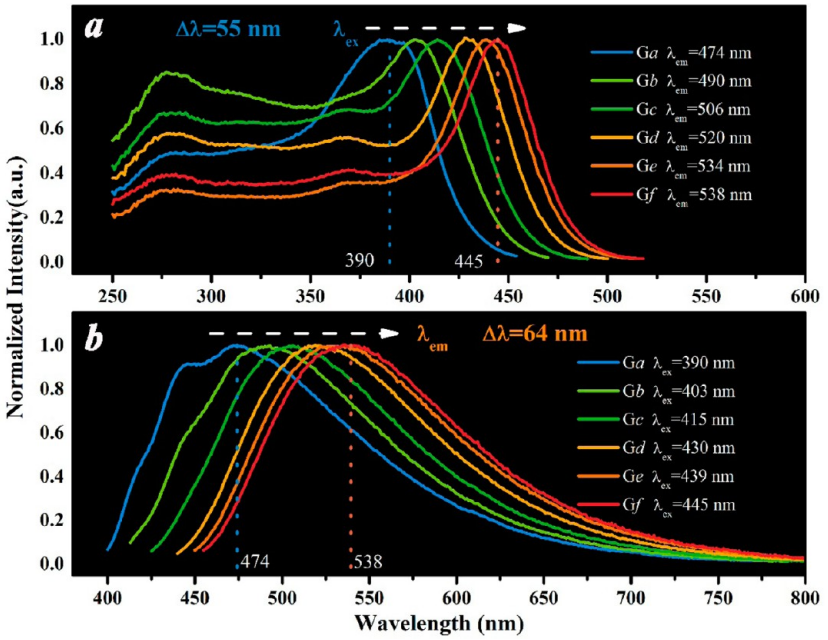

Figure 2. (a) PLE and (b) PL spectra of SLSAKP:xEu^{2+} (x = 0.05, 0.10, 0.20, 0.40, 0.80, and 1.00% for G*a*, G*b*, G*c*, G*d*, G*e*, and G*f*, respectively) glasses.

1.00%). For the host glass SLSAKP, there is only one prominent broadband below 250 nm, which is due to host absorption band. For all the SLSAKP:Eu^{2+} glasses, the absorption spectra are similar to each other and they all have one dominating absorption platform in the wavelength range of 200−450 nm, attributed to the overlapped absorption bands of the host glass below 250 nm and the parity-allowed electric dipole transition, $4f^7(^8S_{7/2}) \rightarrow 4f^65d$,[32,33] of Eu^{2+} above 250 nm. To clearly show pure absorption band of Eu^{2+}, the absorption spectrum of the host glass SLSAKP is subtracted from that of all the SLSAKP:Eu^{2+} glasses as shown in Figure 1b. As the concentration of Eu^{2+} increases, the long-wavelength absorption edge of Eu^{2+} ions shows an obvious red-shift and the absorption intensity gradually increases. The trend is also reflected in the difference in the body color of the obtained glass samples: the host SLSAKP glass is colorless and transparent, and all the SLSAKP:Eu^{2+} glasses have a greenish yellow body color. As an example, the digital photographs of SLSAKP:1.00% Eu^{2+} are shown in the inset in Figure 1b. Furthermore, the body color of the SLSAKP:Eu^{2+} glasses become darker with increasing Eu^{2+} concentration. In general, the gradual red-shift of Eu^{2+} ions transitions in crystalline materials with increasing Eu^{2+} concentration is caused by the increasing crystal field strength of solid-solution compound where Eu^{2+} ions undergo. However, that explanation does not apply to the case of Eu^{2+} in SLSAKP:Eu^{2+} glasses because glass is a kind of noncrystalline material that generally has many local sites with different site environments. Eu^{2+} ions probably occupy one site with low crystal field strength at low concentration of Eu^{2+} ions and another site with high crystal field strength at high Eu^{2+} concentration. Consequently, it leads to the overall gradual red-shift of 4f→5d transitions of Eu^{2+} ions in SLSAKP:Eu^{2+} glasses as the concentration of Eu^{2+} ions increases. Figure 1c shows the normalized difference spectra by subtracting the optical spectra of two SLSAKP:Eu^{2+} glasses with adjacent concentrations of Eu^{2+} shown in Figure 1b. The difference spectra can avoid the overlap effect induced by two adjacent concentrations of Eu^{2+} and clearly show the energy position of the lowest absorption edge of Eu^{2+} ions. With Eu^{2+} concentration increasing, the peaks of difference valves gradually shift to long wavelength, indicating the lowest absorption edge of Eu^{2+} ions shows a red-shift. In other words, Eu^{2+} ions maybe occupy many different sites. As shown in Figure 1d, the long-wavelength absorption edges change from 409 nm for 0.05% Eu^{2+} to 448 nm for 1.00% Eu^{2+} as the dopant concentration increases. Such an obvious and gradual red-shift indicates that Eu^{2+} ions preferentially occupy the site with low crystal field strength and then gradually occupy another site with high crystal field strength in SLSAKP glass as the concentration of Eu^{2+} ions increases.

Figure 2 shows PLE and PL spectra of SLSAKP:xEu^{2+} glass samples. The excitation and emission spectra were recorded at peak wavelength for each sample. It is clearly seen that both PLE and PL spectra of Eu^{2+} show obvious concentration-dependent behavior. At low concentration of Eu^{2+} ions (x = 0.05% for sample G*a*), Eu^{2+} ions exhibit a prominent excitation band at 390 nm and a dominating emission band at 474 nm. As the concentration of Eu^{2+} ions increases, both the excitation and emission bands show an obvious red-shift. At high Eu^{2+} concentration (x = 1.00% for sample G*f*), the excitation and emission bands are dominating at 445 and 538 nm, respectively. Here, the site where Eu^{2+} ions give a shorter wavelength emission is defined as the higher energy site and the site where Eu^{2+} ions give a longer wavelength emission is called as the lower energy site. In general, Eu^{2+} ions give a longer wavelength emission when they undergo stronger crystal field, whereas they exhibit a shorter wavelength emission when they undergo weaker crystal field.[34−36] Consequently, these results suggest that there are rich and distinguishable sites available for Eu^{2+} and that Eu^{2+} ions prefer to occupy higher energy site at low concentration and lower energy site at high concentration, associated with weaker and stronger crystal field, respectively. This explanation is strongly supported by the absorption spectra as shown in Figure 1. As shown in Figure 2 and Figure

DOI: 10.1021/acsami.5b02550
ACS Appl. Mater. Interfaces 2015, 7, 10044−10054

S1 (Supporting Information), the PLE and PL spectra show a red-shift of 55 and 64 nm, respectively. The Stokes shift as a function of Eu^{2+} concentration are also shown in Figure S1 (Supporting Information). The Stokes shift becomes smaller with increasing Eu^{2+} concentration. In SLSAKP:1.00% Eu^{2+} glass, the value of Stokes shift is 3884 cm^{-1}, which is close to that of YAG:Ce^{3+} (3800 cm^{-1}). The full width at half maximum (FWHM) of SLSAKP:$x$$Eu^{2+}$ is within the range 126−134 nm, larger than that of YAG:Ce^{3+} (∼120 nm),[37] which is very important for LG-WLEDs to obtain an improved color rendering index.

More intriguingly, the tunable excitation of SLSAKP:$x$$Eu^{2+}$ glasses makes them match well with the emission of commercial UV-LED chips (300−370 nm), n-UV-LED chips (380−410 nm) or blue-LED chips (420−460 nm), which suggests SLSAKP:$x$$Eu^{2+}$ glasses can be expected to be a potential luminescent glass convertor for LED devices. Moreover, Eu^{2+} ions give a tunable emission as their concentration increases. The CIE color coordinates of the SLSAKP:$x$$Eu^{2+}$ glasses are shown in Figure S2 (Supporting Information). It is clearly seen that the color hues of the samples change from blue-white to green and finally even to yellowish-green as shown in the inset photographs under Xe lamp excitation. In summary, we obtain excitation- and emission-on-demand glasses for white LEDs by simply adjusting concentration of Eu^{2+} ions in SLSAKP glass.

Quantum efficiency (QE) is an important parameter for luminescent materials indicating to what extent it can be practically used. For glassy materials, external quantum efficiency (EQE) changes as the optical route (glass thickness) varies. Thus, internal quantum efficiency (IQE) is typically used to characterize its luminescent properties.[38−40] As an illustration, the excitation line and the emission spectrum of the SLSAKP:0.40% Eu^{2+} glass sample are shown in Figure S3 (Supporting Information). The measured IQE of SLSAKP:-$x$$Eu^{2+}$ glasses are listed in Table 1. Obviously, the IQE

Table 1. CIE 1931 Color Coordinates and IQE of SLSAKP: $x$$Eu^{2+}$ Glasses

Eu^{2+} concentration (mol %)	λ_{ex} (nm)	CIE 1931 color coordinates		IQE (%)
		CIE x	CIE y	
0.05	390	0.228	0.289	16
0.10	403	0.251	0.358	17
0.20	415	0.285	0.431	16
0.40	430	0.331	0.497	14
0.80	439	0.360	0.518	10
1.00	445	0.377	0.528	9

decreases as the concentration of Eu^{2+} increases. Eu^{2+} ions show relatively high IQE of about 16% at low concentration and low IQE of about 10% at high concentration. These results suggest that Eu^{2+} ions at higher energy site exhibit more efficient emission than they at lower energy site. Compared with the crystalline materials, the IQE values of $x$$Eu^{2+}$-doped SLSAKP glasses are not high enough, mainly due to high phonon energy and flabby coordination environment in glasses.

It is also interesting that Eu^{2+} ions show the excitation wavelength-dependent tunable emission performance besides the concentration-dependent tunable emission properties discussed above. Figure 3 typically exhibits the PL spectra of SLSAKP:$x$$Eu^{2+}$ glasses (x = 0.05, 0.40, and 1.00%) under continuous excitation wavelengths with a step of 10 nm. For x = 0.05%, Eu^{2+} ions give a tunable emission with a gradual red-shift of about 66 nm, the intensity of which initially increases and then decreases, when the excitation wavelength varies from 360 to 450 nm. Such dependence of the integrated intensity and emission peak wavelength on excitation wavelength is clearly displayed in Figure 3(a***). Similarly, the other two glasses show almost the same behavior. The difference is that the red-shift is about 66 nm for x = 0.05%, 44 nm for x = 0.40% and 36 nm for x = 1.00% and the optimal excitation wavelength is about 390 nm for x = 0.05%, 430 nm for x = 0.40% and 445 nm for x = 1.00%. The reason why Eu^{2+} ions show the excitation wavelength-dependent tunable emission performance at fixed concentration is that rich and distinguishable sites in SLSAKP glasses are occupied by Eu^{2+} at whatever low or high concentration even if Eu^{2+} ions preferentially occupy high energy site at low concentration and then gradually occupy low energy site at high concentration. In addition, it is obviously seen that the red-shift of emission decreases with increasing Eu^{2+} concentration, which is ascribed to the emission quenching of Eu^{2+} ions at the high energy site by reabsorbing of Eu^{2+} at the low energy site as shown in Figure S4 (Supporting Information). This explanation is strongly supported by the lifetime data of Eu^{2+}. As shown in Figure S4 (Supporting Information), the lifetime of Eu^{2+} at the same site (λ_{ex} = 390 nm, λ_{em} =474 nm) decreases from 1.14 μs (0.05% Eu^{2+}) to 0.97 μs (1.00% Eu^{2+}), suggesting that energy transfer happens from Eu^{2+} ions at high energy site to Eu^{2+} at low energy site. Consequently, the emission of Eu^{2+} at high energy site is quenched in glasses with high concentration of Eu^{2+} ions.

Figure 4 shows the CIE chromaticity diagram and the photographs of SLSAKP:Eu^{2+} glasses under continuous excitation wavelengths with a step of 10 nm. The excitation light is supplied by the Xe lamp of the FSP920. It is obviously seen that the emitting color and CIE color coordinates of Eu^{2+} ions are finely tunable in excitation wavelength range from 360 to 450 nm. For x = 0.05%, Eu^{2+} ions give an intense cyan emission (λ_{ex} = 360−410 nm), weak green emission (λ_{ex} = 420−430 nm) and poor yellowish-green emission (λ_{ex} > 430 nm). Accordingly, the CIE coordinates vary greatly from (0.228, 0.287) to (0.377, 0.521). For x = 0.40%, Eu^{2+} ions emit an intense and tunable light from green (λ_{ex} = 360−410 nm) to yellowish-green emission (λ_{ex} = 420−450 nm). At the meantime, the CIE coordinates change from (0.283, 0.446) to (0.384, 0.526). For x = 1.0%, Eu^{2+} ions give an intense and tunable emission from green (λ_{ex} = 360−410 nm) to yellowish-green (λ_{ex} = 420−450 nm) and the CIE coordinates shift gradually from (0.303, 0.492) to (0.389, 0.530). In conclusion, we have two simple approaches to obtain excitation- and emission-on-demand glasses for white LEDs: one approach is to change the excitation wavelength and the other is to adjust the concentration of Eu^{2+} ions in SLSAKP.

To prove the existence of rich and distinguishable sites available for Eu^{2+} ions in the glass, we measured the dependence of the lifetime of Eu^{2+} on its concentration and excitation wavelength and these results are shown in Figure 5. All the decay curves can be well-fitted with a second-order exponential equation[41,42]

$$I = A_1\exp(-t/\tau_1) + A_2\exp(-t/\tau_2) \quad (1)$$

where I is the luminescence intensity, A_1 and A_2 are constants, t is the lifetime, and τ_1 and τ_2 are rapid and slow lifetimes for

DOI: 10.1021/acsami.5b02550
ACS Appl. Mater. Interfaces 2015, 7, 10044−10054

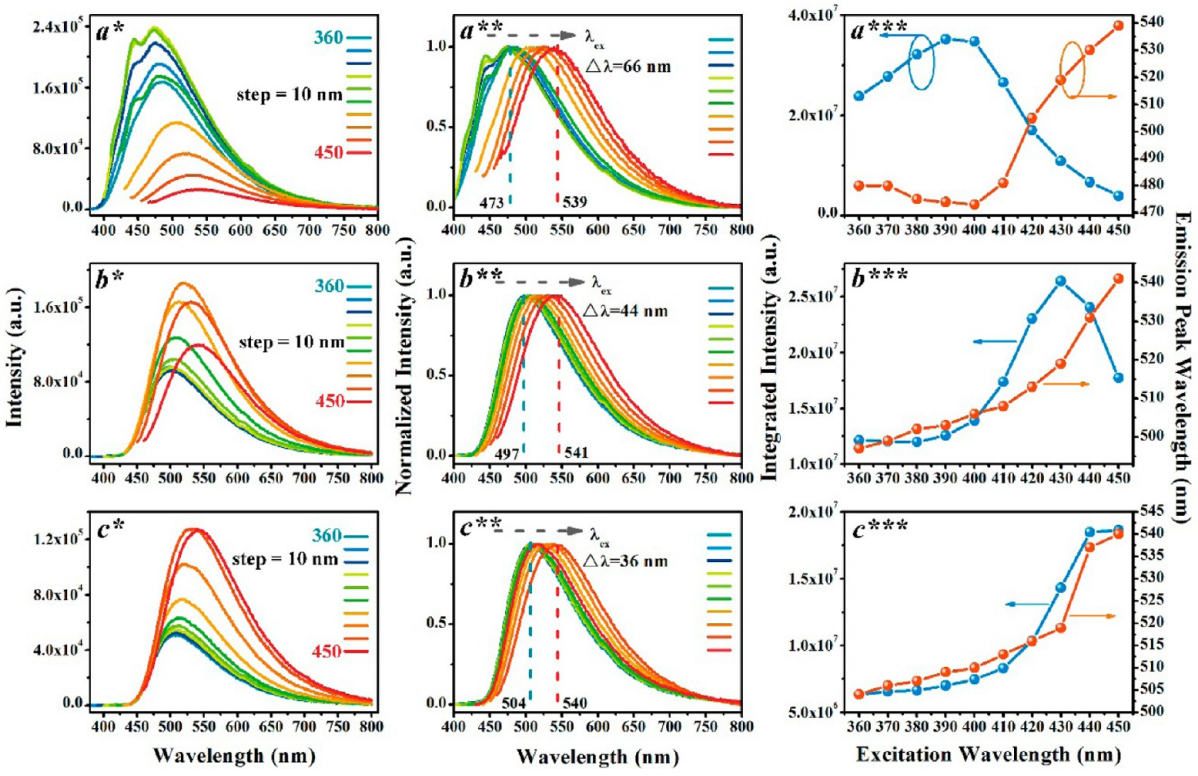

Figure 3. Non-normalized (*), normalized (**) PL spectra and the excitation wavelength-dependent emission performance (***) of (a) SLSAKP:0.05% Eu^{2+}, (b) SLSAKP:0.40% Eu^{2+}, and (c) SLSAKP:1.00% Eu^{2+} glass samples under different excitation wavelengths ranging from 360 to 450 nm.

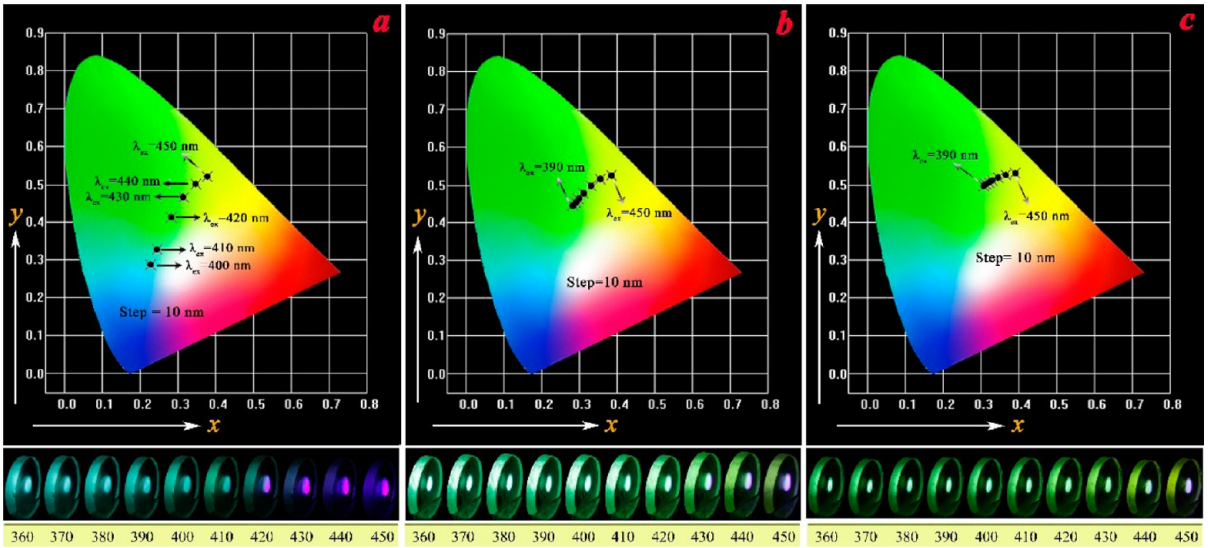

Figure 4. CIE chromaticity diagram and photographs of SLSAKP:xEu^{2+} (x = (a) 0.05%, (b) 0.40%, and (c) 1.00%) glasses under continuous excitation wavelengths with a step of 10 nm.

exponential components, respectively. The average lifetime (τ^*) can be determined by the formula given in the following:

$$\tau^* = (A_1\tau_1^2 + A_2\tau_2^2)/(A_1\tau_1 + A_2\tau_2) \quad (2)$$

As shown in Figure 5a–f, the average lifetimes of Eu^{2+} exhibit obvious concentration dependence. It gradually increases from 1.14 μs for x = 0.05% to 1.56 μs for x = 1.00%. Obviously, Eu^{2+} at the high energy site has a short lifetime and the one at the low energy site has a long lifetime. These results suggest that the local site environment available for Eu^{2+} ions is quite different as the concentration of Eu^{2+} ions increases. Figure 5g shows the decay curves of SLSAKP:1.00% Eu^{2+} glass monitored at different excitation and emission wavelengths. It is clearly seen that the lifetimes of Eu^{2+} at fixed concentration show obvious excitation wavelength dependence. Similarly, it gradually increases as the excitation wavelength continuously varies from 390 to 445 nm. These results indicate that at fixed concentration, Eu^{2+} ions occupy lots of distinguishable local sites in SLSAKP glasses.

DOI: 10.1021/acsami.5b02550
ACS Appl. Mater. Interfaces 2015, 7, 10044–10054

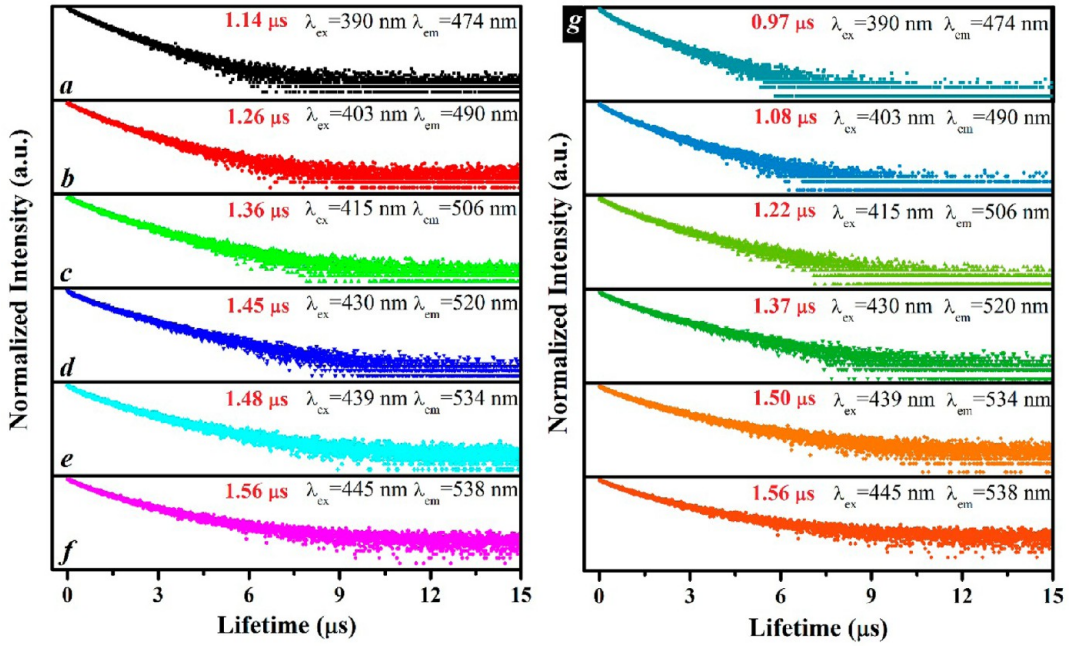

Figure 5. Decay curves of SLSAKP:xEu^{2+} (x = 0.05, 0.10, 0.20, 0.40, 0.80, and 1.00% for a–f, respectively) glasses and (g) decay curves of SLSAKP:1.00% Eu^{2+} glass monitored at different excitation and emission wavelengths.

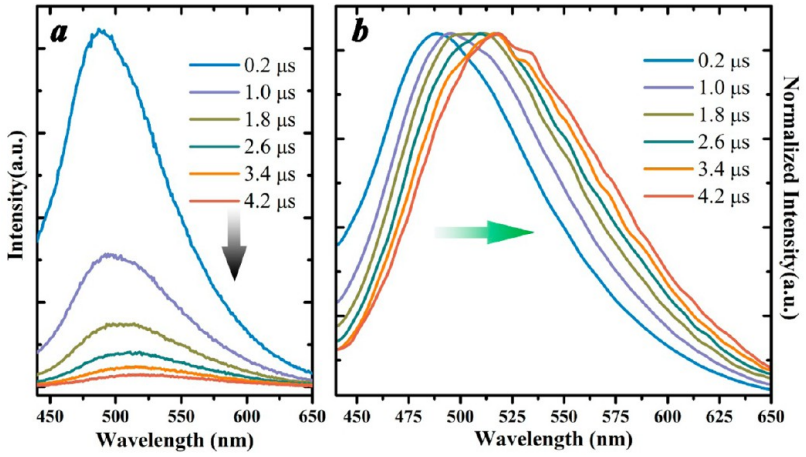

Figure 6. (a) Non-normalized and (b) normalized time-resolved emission spectra (TRES) of sample SLSAKP:1.00% Eu^{2+} (λ_{ex} = 370 nm).

To obtain further proof for the existence of rich and distinguishable sites available for Eu^{2+} ions in the glass, time-resolved emission spectra (TRES) of sample SLSAKP:1.00% Eu^{2+} were measured at RT temperature, as shown in Figure 6. As delay time increases, it is obviously seen that emission intensity decreases gradually and at the same time the emission spectra show a red-shift of about 40 nm. As clearly seen in normalized TRES (Figure 6b), the emission is prominent at 480, 502, 512, and 520 nm at a delay time of 0.2, 1.8, 2.6, and 4.2 μs, respectively.

In summary, all the time-resolved PL data including the decay curves and TRES give a strong evidence for the existence of rich and distinguishable local sites available for Eu^{2+} ions in glasses, which are accordance with the steady-state PLE and PL data discussed above.

Thermal quenching behavior, as one of the important parameters, is required to be considered and investigated for high-power white LEDs applications. Figure 7 shows the temperature-dependent PL spectral emission of SLSAKP:0.05% Eu^{2+} upon 360 nm excitation (a), SLSAKP:0.40% Eu^{2+} upon 410 nm excitation (b), and SLSAKP:1.00% Eu^{2+} upon 450 nm excitation (c). As the temperature increases, the PL intensities of Eu^{2+} decrease rapidly. Figure 8a shows the relative integrated intensity dependence of temperature. For SLSAKP:0.05% Eu^{2+} glass, at 373 and 423 K, it is only about 70.45% and 51.12% of the initial intensity at 298 K under 360 nm excitation, respectively. The relative integrated intensity decreases from initial 100% at 298 K to 64.87% at 373 K and 46.55% at 423 K, respectively, in SLSAKP:0.40% Eu^{2+} glass sample. For SLSAKP:1.00% Eu^{2+} glass, the integrated intensities at 373 and 423 K are 72.3% and 53.38% of the initial value at 298 K, respectively. Such serious thermal quenching behavior may be caused by smaller activation energy. In general, the smaller activation energy is, the poorer thermal quenching behavior is. The thermal quenching data of the SLSAKP:0.05% Eu^{2+}, SLSAKP:0.40% Eu^{2+}, and SLSAKP:1.00% Eu^{2+} glasses were fitted using the following Arrhenius equation to calculate the activation energy[43,44]

DOI: 10.1021/acsami.5b02550
ACS Appl. Mater. Interfaces 2015, 7, 10044–10054

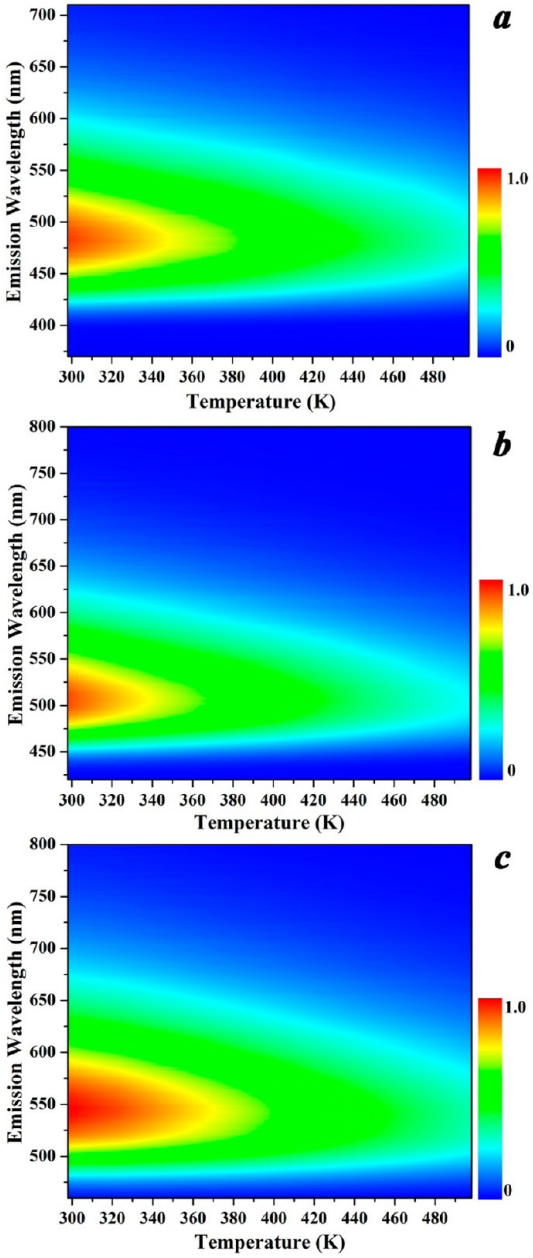

Figure 7. Temperature dependence of the spectral emission of (a) SLSAKP:0.05% Eu^{2+} upon 360 nm excitation, (b) SLSAKP:0.40% Eu^{2+} upon 410 nm excitation, and (c) SLSAKP:1.00% Eu^{2+} upon 450 nm excitation.

$$I_T = \frac{I_0}{1 + A\exp\left(-\frac{E_a}{k_B T}\right)} \quad (3)$$

In eq 3, I_0 is the initial emission intensity, I_T is the intensity at different temperatures, E_a is activation energy of thermal quenching, A is a constant, and k_B is the Boltzmann constant (8.617×10^{-5} eV/K). The E_a for SLSAKP:0.05% Eu^{2+}, SLSAKP:0.40% Eu^{2+}, and SLSAKP:1.00% Eu^{2+} glasses were determined to be ~0.2298, ~0.2264, and ~0.2494 eV under excitation of 360, 410, and 450 nm, respectively, which are presented in Figure 8b. Therefore, it is reasonable that Eu^{2+} ions show more serious thermal quenching behavior in SLSAKP:0.40% Eu^{2+} glass than that in SLSAKP:0.05% Eu^{2+} glass and SLSAKP:1.00% Eu^{2+} glass.

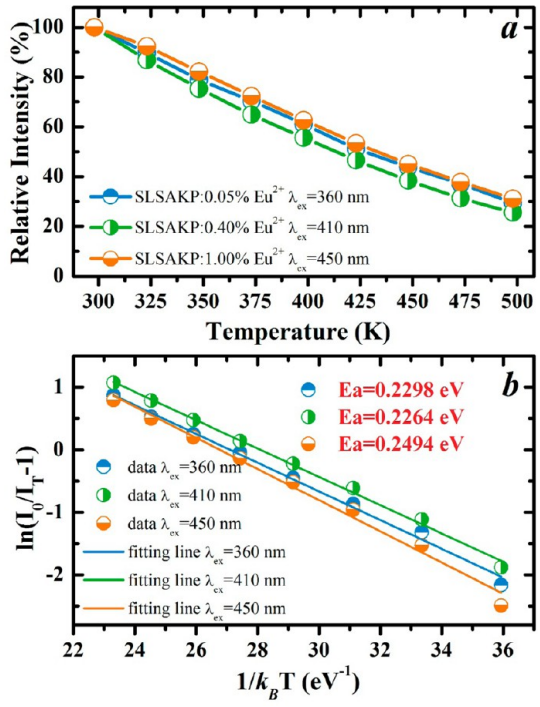

Figure 8. (a) PL integrated intensity as a function of temperature; (b) Arrhenius fitting thermal quenching and the calculated activation energy (E_a) of SLSAKP:0.05% Eu^{2+}, SLSAKP:0.40% Eu^{2+}, and SLSAKP:1.00% Eu^{2+}.

To be applied in high-power white LEDs with high stable white light quality, it is very important for luminescent materials to have high optical stability at high joint-temperature of LED chip. To evaluate the color stability of the glasses under high joint-temperature of LED chip, the CIE color coordinates and CIE shift (ΔE) with increasing temperature are shown in Figure 9 and Table 2. It is clearly seen in Figure 9 that all the

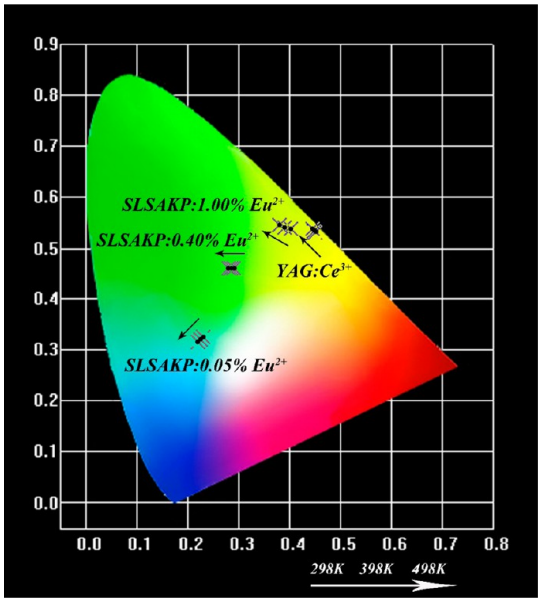

Figure 9. CIE chromaticity coordinates at different temperatures for the SLSAKP:0.05% Eu^{2+} upon 360 nm excitation, SLSAKP:0.40% Eu^{2+} upon 410 nm excitation, SLSAKP:1.00% Eu^{2+} upon 450 nm excitation, and commercial YAG:Ce^{3+} phosphor upon 450 nm excitation.

DOI: 10.1021/acsami.5b02550
ACS Appl. Mater. Interfaces 2015, 7, 10044−10054

Table 2. Chromaticity Shift (ΔE) of SLSAKP:0.05% Eu^{2+}, SLSAKP:0.40% Eu^{2+}, SLSAKP:1.00% Eu^{2+}, and Commercial YAG:Ce^{3+} Phosphor as A Function of Temperature

	λ_{ex} (nm)	298 K	398 K	498 K	ref
SLSAKP:0.05% Eu^{2+}	360		7.8×10^{-3}	13.8×10^{-3}	this work
SLSAKP:0.40% Eu^{2+}	410		5.2×10^{-3}	7.8×10^{-3}	this work
SLSAKP:1.00% Eu^{2+}	450		12.0×10^{-3}	19.7×10^{-3}	this work
commercial YAG:Ce^{3+}	450		4.3×10^{-3}	6.3×10^{-3}	this work
commercial white-emitting phosphor mixture	370		20.4×10^{-3}	51.4×10^{-3}	46

SLSAKP:Eu^{2+} glasses show good color stability comparable to commercial YAG:Ce^{3+} phosphor, which is consistent with the normalized temperature-dependent emission spectra of SLSAKP:Eu^{2+} as shown in Figure S5 (Supporting Information). To quantitatively describe the color stability, the chromaticity shift (ΔE) was calculated using the following equation[45,46]

$$\Delta E = \sqrt{(u'_t - u'_o)^2 + (v'_t - v'_o)^2 + (w'_t - w'_o)^2} \quad (4)$$

where $u' = 4x/(3 - 2x + 12y)$, $v' = 9y/(3 - 2x + 12y)$ and $w' = 1 - u' - v'$. u' and v' are the chromaticity coordinates in $u'v'$ uniform color space, x and y are the chromaticity coordinates in CIE 1931 color space, and o and t are the chromaticity shift at 298 K and a given temperature, respectively. As shown in Table 2, all the glasses doped with 0.05, 0.40, and 1.00% Eu^{2+} show that the chromaticity shift increases gradually with increasing temperature. Among them, the SLSAKP:0.40% Eu^{2+} glass shows the best performance and its chromaticity shift is about 5.2×10^{-3} and 7.8×10^{-3} at 398 and 498 K, respectively, which is only about one-fourth and one-fifth of the commercial white-emitting phosphor mixture.[46] These results demonstrate that it is a potential luminescent glass for high-quality white LEDs based on high-power n-UV LED chip. For the SLSAKP:1.00% Eu^{2+} glass, its chromaticity shift is about 12.0×10^{-3} and 19.7×10^{-3} at 398 and 498 K, respectively, which is about 3 times of the commercial YAG:Ce^{3+} phosphor. These results indicate that it is not an ideal luminescent glass for high-quality white LEDs based on high-power blue LED chip.

3.2. Potential Application of SLSAKP:Eu^{2+} Glasses. As discussed above, we obtained tunable excitation/emission SLSAKP:Eu^{2+} glasses with potential applications for white LEDs by two simple approaches: one approach is to selectively excite Eu^{2+} ions at different local sites and the other is to adjust the concentration of Eu^{2+} ions. To demonstrate the potential application of SLSAKP:Eu^{2+} glasses, we representatively chose SLSAKP:1.0% Eu^{2+} glass to fabricate an LG-LED device based on 385 nm n-UV COB and 450 nm blue COB, as illustrated in Figures 10 and 12, respectively. The glass was rough-polished in order to obtain homogeneous emitting light that is hard to realize by traditional phosphors slurry, which can be clearly seen in Figure 10a–c. Figure 10d shows the LG-LED device prototype. The n-UV COB was fixed on the aluminum sink and a plate of the SLSAKP:1.0% Eu^{2+} glass was simply placed on it. Driven by 100 mA current, the LG-LED device prototype emits intense and uniform green light with the color coordinates (0.346, 0.506), as shown in the CIE chromaticity diagram in Figure 11c. Figure 11a, b shows the spectra of naked n-UV

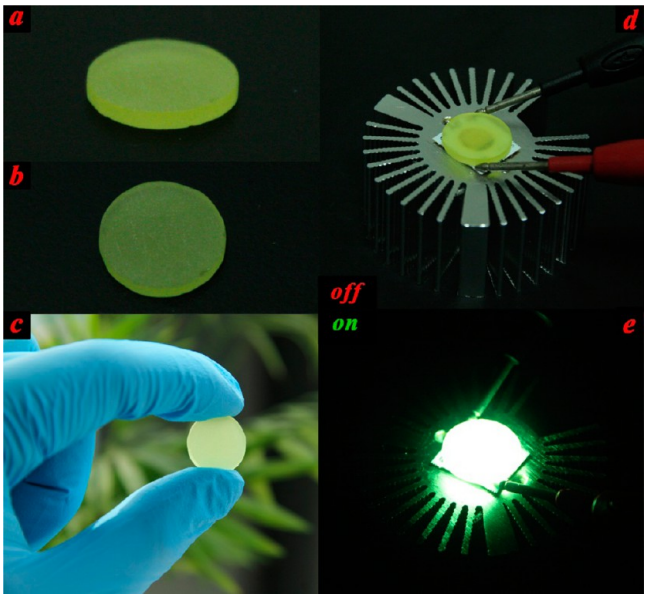

Figure 10. (a–c) Photographs of SLSAKP:1.0% Eu^{2+} glass; (d) photograph of the fabricated LG-LED device and (e) photograph of LG-LED device driven by 100 mA current.

COB and green LG-LED device. It is obviously seen that naked n-UV COB chip gives a dominating emission at 385 nm and LG-LED device exhibits an intense green broadband emission centering at 525 nm and covering from 450 to 750 nm. Moreover, it can be carefully seen in Figure 11b that the green LG-LED device shows a much weaker n-UV light intensity when compared to previous report.[47−49] These results indicate that this luminescent glass has strong n-UV absorption efficiency and higher down-converting efficiency. It is vital for LED device to prevent the n-UV light from leaking out since the n-UV is harmful to human body. All these results indicate that the SLSAKP:Eu^{2+} glass is suitable for n-UV LED to obtain a green light in LG-LED device.

Besides the n-UV COB, blue COB was also employed to fabricate the LG-LED device. As shown in Figure 12c, d, the LG-LED device gives a bluish white light because of the scarcity of red emission. Accordingly, the color coordinates and CCT of the LG-LED device are (0.261, 0.255) and 17507 K, as presented in Figure 13e. To obtain the pure white light, we employed PiG technology. $CaAlSiN_3$:Eu^{2+}, as a famous commercial red phosphor, was used to obtain red-emitting PiG plate to enhance the blue light absorption and decrease the CCT of the LED device. The $CaAlSiN_3$:Eu^{2+}-based PiG was simply stacked on the SLSAKP:Eu^{2+} glass, as shown in Figure 12e. Under an operating current of 100 mA, this LG-LED device generates a white light, purer than the SLSAKP:Eu^{2+} glass, as shown in Figures 12f and 13e, because of the enhancement of red emission from red-emitting PiG (Figure 13d). And the color coordinates and CCT of this LG-WLED are (0.327, 0.333) and 5749 K. All these results demonstrate that the tunable emission SLSAKP:Eu^{2+} glass can be used for both UV-LED- and blue-LED-based LED devices. But one should keep in mind that the quantum efficiencies of the SLSAKP:Eu^{2+} glasses are still not high enough (Table 1). Therefore, further work should be done in order to achieve practically acceptable quantum efficiencies of the as synthesized glasses in the near future. Glass-ceramic[50] or PiG[30,31,51]

DOI: 10.1021/acsami.5b02550
ACS Appl. Mater. Interfaces 2015, 7, 10044−10054

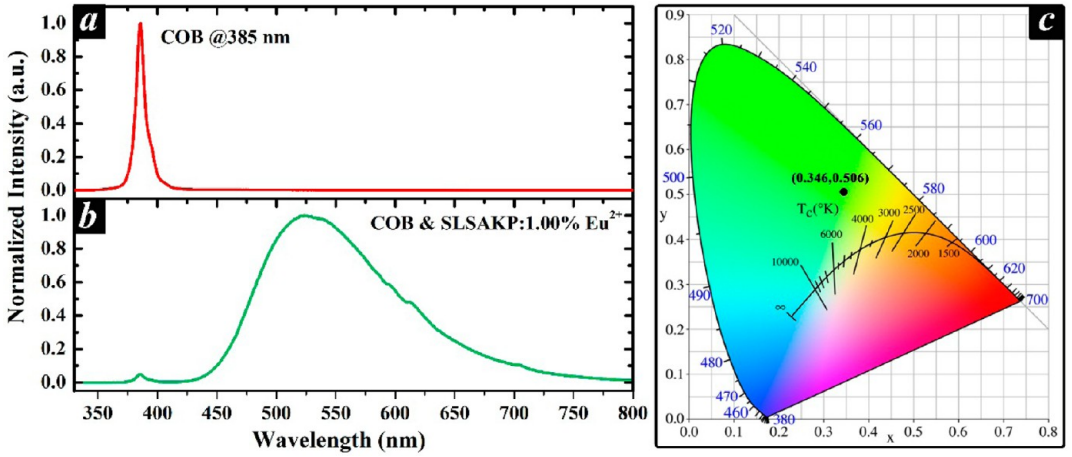

Figure 11. (a, b) EL spectra and (c) CIE chromaticity coordinates of the as-fabricated green-emitting LG-LED device combined SLSAKP:1.0% Eu^{2+} glass and n-UV-COB under an operating current of 100 mA.

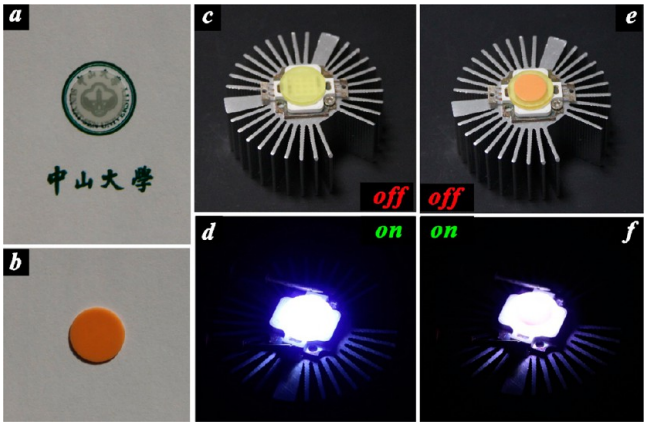

Figure 12. (a, b) Photographs of glass plate without and with red phosphor $CaAlSiN_3:Eu^{2+}$; photographs of (c, e) the LG-LED devices and (d, f) the lamps in operation.

technique would be a promising choice to obtain luminescent crystalline particles, which uniformly disperse in glass host.

4. CONCLUSION

In conclusion, widely and continuously tunable emitting light are successfully achieved via site engineering in Eu^{2+} ion-doped glass. The absorption spectra, PLE and PL spectra, and decay curves reveal there are rich and distinguishable local cation sites in SLASKP glasses and that Eu^{2+} ions show preferable site distribution, which offer the possibility to engineer the local site environment available for Eu^{2+} ions. The site engineering consequently contributes to emission-on-demand simply by changing excitation wavelength and adjusting the concentration of Eu^{2+} ions. Such widely and continuously tunable photoluminescence performance in glasses is a rare but desirable characteristic that is not present in crystalline materials. The COB-based color and white LED devices were successfully

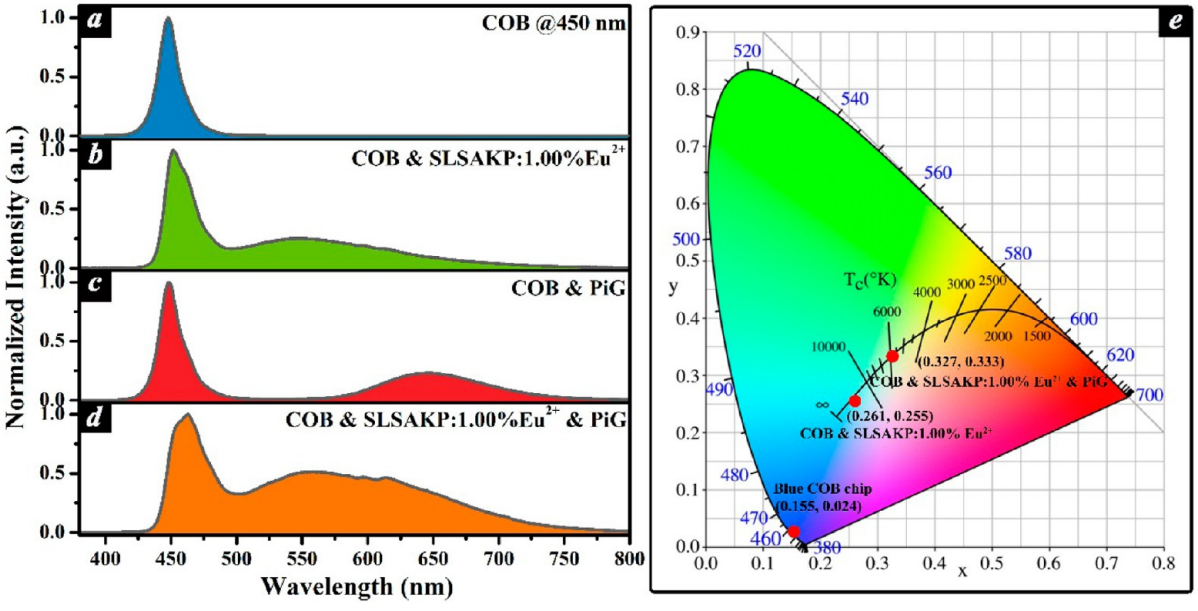

Figure 13. EL spectra of (a) blue COB chip, (b) blue COB chip and SLSAKP:1.0% Eu^{2+} glass, (c) blue COB chip and $CaAlSiN_3:Eu^{2+}$-based PiG, and (d) blue COB chip and SLSAKP:1.0% Eu^{2+} glass and $CaAlSiN_3:Eu^{2+}$-based PiG; (e) CIE coordinates of the as-fabricated LG-LED devices.

DOI: 10.1021/acsami.5b02550
ACS Appl. Mater. Interfaces 2015, 7, 10044−10054

fabricated, which demonstrates the potential application of site engineering in advanced solid-state lighting in the future.

■ ASSOCIATED CONTENT

Supporting Information

The maximum excitation wavelength, maximum emission wavelength, and Stokes shift as a function of Eu^{2+} concentration (Figure S1). CIE chromaticity coordinates diagram of xEu^{2+}-doped SLSAKP glasses and the corresponding emitting color photographs (Figure S2). Spectra of the excitation light and emission spectra of SLSAKP:0.40% Eu^{2+} glass collected by using an integrating sphere (Figure S3). Normalized PLE spectrum of the SLSAKP:1.00% Eu^{2+} and PL spectrum of the SLSAKP:0.05% Eu^{2+} and decay curves of the same site in the SLSAKP:1.00% Eu^{2+} and SLSAKP:0.05% Eu^{2+} (Figure S4). Normalized temperature-dependent emission spectra of the SLSAKP:0.05% Eu^{2+}, SLSAKP:0.40% Eu^{2+}, SLSAKP:1.00% Eu^{2+} and commercial YAG:Ce^{3+} phosphor (Figure S5). The Supporting Information is available free of charge on the ACS Publications website at DOI: 10.1021/acsami.5b02550.

■ AUTHOR INFORMATION

Corresponding Author

*E-mail: ceswj@mail.sysu.edu.cn. Tel: +86-20-84112112. Fax: +86-20-84111038.

Notes

The authors declare no competing financial interest.

■ ACKNOWLEDGMENTS

This work was financially supported by the "973" programs (2014CB643801), the NSFC (21271191), the Joint Funds of the National Natural Science Foundation of China and Guangdong Province (U1301242), Teamwork Projects of Guangdong Natural Science Foundation (S2013030012842), Guangdong Provincial Science & Technology Project (2013B090800019 and 2013Y2-00118), Natural Science Foundation of Guangdong Province (2014A030313114), China Postdoctoral Science Foundation (2014M562237), and the Fundamental Research Funds for the Central Universities (14lgqt02).

■ REFERENCES

(1) Deng, R.; Qin, F.; Chen, R.; Huang, W.; Hong, M.; Liu, X. Temporal Full-Colour Tuning through Non-Steady-State Upconversion. *Nat. Nanotechnol.* **2015**, *10*, 237−242.

(2) Pradhan, N.; Goorskey, D.; Thessing, J.; Peng, X. An Alternative of CdSe Nanocrystal Emitters: Pure and Tunable Impurity Emissions in ZnSe Nanocrystals. *J. Am. Chem. Soc.* **2005**, *127*, 17586−17587.

(3) Pollock, J. B.; Schneider, G. L.; Cook, T. R.; Davies, A. S.; Stang, P. J. Tunable Visible Light Emission of Self-Assembled Rhomboidal Metallacycles. *J. Am. Chem. Soc.* **2013**, *135*, 13676−13679.

(4) Medintz, I. L.; Uyeda, H. T.; Goldman, E. R.; Mattoussi, H. Quantum Dot Bioconjugates for Imaging, Labelling and Sensing. *Nat. Mater.* **2005**, *4*, 435−446.

(5) Shang, M.; Li, C.; Lin, J. How to Produce White Light in A Single-Phase Host? *Chem. Soc. Rev.* **2014**, *43*, 1372−1386.

(6) Kuykendall, T.; Ulrich, P.; Aloni, S.; Yang, P. Complete Composition Tunability of InGaN Nanowires Using a Combinatorial Approach. *Nat. Mater.* **2007**, *6*, 951−956.

(7) Gai, S.; Li, C.; Yang, P.; Lin, J. Recent Progress in Rare Earth Micro/Nanocrystals: Soft Chemical Synthesis, Luminescent Properties and Biomedical Applications. *Chem. Rev.* **2014**, *114*, 2343−2389.

(8) Zhou, S.; Jiang, N.; Wu, B.; Hao, J.; Qiu, J. Ligand-Driven Wavelength-Tunable and Ultra- Broadband Infrared Luminescence in Single-Ion-Doped Transparent Hybrid Materials. *Adv. Funct. Mater.* **2009**, *19*, 2081−2088.

(9) Dhanaraj, J.; Jagannathan, R.; Trivedi, D. C. $Y_2O_2S:Eu^{3+}$ Nanocrystals-Synthesis and Luminescent Properties. *J. Mater. Chem.* **2003**, *13*, 1778−1782.

(10) Kandarakis, I.; Cavouras, D.; Panayiotakis, G. S.; Nomicos, C. D. Evaluating X-ray Detectors for Radiographic Applications: A Comparison of ZnSCdS:Ag with Gd_2O_2S:Tb and Y_2O_2S:Tb Screens. *Phys. Med. Biol.* **1997**, *42*, 1351−1373.

(11) Feldmann, C.; Jüstel, T.; Ronda, C. R.; Schmidt, P. J. Inorganic Luminescent Materials: 100 Years of Research and Application. *Adv. Funct. Mater.* **2003**, *13*, 511−516.

(12) Li, G.; Geng, D.; Shang, M.; Peng, C.; Cheng, Z.; Lin, J. Tunable Luminescence of Ce^{3+}/Mn^{2+}-Coactivated $Ca_2Gd_8(SiO_4)_6O_2$ through Energy Transfer and Modulation of Excitation: Potential Single-Phase White/Yellow-Emitting Phosphors. *J. Mater. Chem.* **2011**, *21*, 13334−13344.

(13) Lacanilao, A.; Wallez, G.; Mazerolles, L.; Buissette, V.; Mercier, T. L.; Aurissergues, F.; Trichet, M.-F.; Dupré, N.; Pavageau, B.; Servant, L.; Viana, B. A Structural Approach of the Flux Effect on Blue Phosphor BAM:Eu ($BaMgAl_{10}O_{17}:Eu^{2+}$). *Mater. Res. Bull.* **2013**, *48*, 2960−2968.

(14) Wang, Z. L.; Cheah, K. W.; Tam, H. L.; Gong, M. L. Near-Ultraviolet Light Excited Deep Blue-Emitting Phosphor for Solid-State Lighting. *J. Alloys Compd.* **2009**, *482*, 437−439.

(15) Brgoch, J.; Gaultois, M. W.; Balasubramanian, M.; Page, K.; Hong, B.-C.; Seshadri, R. Local Structure and Structural Rigidity of the Green Phosphor β-SiAlON:Eu^{2+}. *Appl. Phys. Lett.* **2014**, *105*, 181904.

(16) Hirosaki, N.; Xie, R.-J.; Kimoto, K.; Sekiguchi, T.; Yamamoto, Y.; Suehiro, T.; Mitomo, M. Characterization and Properties of Green-Emitting β-SiAlON:Eu^{2+} Powder Phosphors for White Light-Emitting Diodes. *Appl. Phys. Lett.* **2005**, *86*, 211905.

(17) Niu, J.; Saito, G.; Akiyama, T. A New Route to Synthesize β-SiAlON:Eu^{2+} Phosphors for White Light-Emitting Diodes. *Appl. Phys. Express* **2013**, *6*, 042105.

(18) Nersisyan, H.; Won, H. I.; Won, C. W. Highly Effective Synthesis and Photoluminescence of $Sr_2Si_5N_8:Eu^{2+}$ Red-Emitting Phosphor for LEDs. *Chem. Commun.* **2011**, *47*, 11897−11899.

(19) Zeuner, M.; Schmidt, P. J.; Schnick, W. One-Pot Synthesis of Single-Source Precursors for Nanocrystalline LED Phosphors $M_2Si_5N_8:Eu^{2+}$ (M = Sr, Ba). *Chem. Mater.* **2009**, *21*, 2467−2473.

(20) Xie, R.-J.; Hirosaki, N.; Suehiro, T.; Xu, F.-F.; Mitomo, M. A simple, Efficient Synthetic Route to $Sr_2Si_5N_8:Eu^{2+}$-Based Red Phosphors for White Light-Emitting Diodes. *Chem. Mater.* **2006**, *18*, 5578−5583.

(21) Yeh, C.-W.; Chen, W.-T.; Liu, R.-S.; Hu, S.-F.; Sheu, H.-S.; Chen, J.-M.; Hintzen, H. T. Origin of Thermal Degradation of $Sr_{2-x}Si_5N_8:Eu_x$ Phosphors in Air for Light-Emitting Diodes. *J. Am. Chem. Soc.* **2012**, *134*, 14108−14117.

(22) Sato, Y.; Kato, H.; Kobayashi, M.; Masaki, T.; Yoon, D.-H.; Kakihana, M. Tailoring of Deep-Red Luminescence in Ca_2SiO_4: Eu^{2+}. *Angew. Chem., Int. Ed.* **2014**, *53*, 7756−7759.

(23) Kawano, Y.; Kim, S. W.; Ishigaki, T.; Uematsu, K.; Toda, K.; Takaba, H.; Sato, M. Site Engineering Concept of Ce^{3+}-Activated Novel Orange-Red Emission Oxide Phosphors. *Opt. Mater. Express* **2014**, *4*, 1770−1774.

(24) Zhang, J.; Jiang, C. Luminescence Properties of $Ca_{14}Mg_2(SiO_4)_8:Eu^{2+}$ from Various Eu^{2+} Sites for White-Light-Emitting Diodes. *Mater. Res. Bull.* **2014**, *60*, 467−473.

(25) Kim, T.-G.; Kim, T.; Kim, J.; Kim, S.-J.; Im, S.-J. Interplay between Crystal Structure and Photoluminescence Properties of β-$Ca_3SiO_4Cl_2:Eu^{2+}$. *J. Phys. Chem. C* **2014**, *118*, 12428−12435.

(26) Zhou, S.; Guo, Q.; Inoue, H.; Ye, Q.; Masuno, A.; Zheng, B.; Yu, Y.; Qiu, J. Topological Engineering of Glass for Modulating Chemical State of Dopants. *Adv. Mater.* **2014**, *26*, 7966−7972.

(27) Eichelbaum, M.; Rademann, K. Plasmonic Enhancement or Energy Transfer? On the Luminescence of Gold-, Silver-, and Lanthanide-Doped Silicate Glasses and Its Potential for Light-Emitting Devices. *Adv. Funct. Mater.* **2009**, *19*, 2045−5252.

DOI: 10.1021/acsami.5b02550
ACS Appl. Mater. Interfaces 2015, 7, 10044−10054

(28) Andrade, L. H. C.; Lima, S. M.; Baesso, M. L.; Novatski, A.; Rohling, J. H.; Guyot, Y.; Boulon, G. Tunable Light Emission and Similarities with Garnet Structure of Ce-doped LSCAS Glass for White-Light Devices. *J. Alloys Compd.* **2012**, *510*, 54−59.
(29) Lima, S. M.; Andrade, L. H. C.; Rocha, A. C. P.; Silva, J. R.; Farias, A. M.; Medina, A. N.; Baesso, M. L.; Nunes, L. A. O.; Guyot, Y.; Boulon, G. Eu^{2+}-Doped OH-Free Calcium Aluminosilicate Glass: A Phosphor for Smart Lighting. *J. Lumin.* **2013**, *143*, 600−604.
(30) Lee, J. S.; Unithrattil, S.; Kim, S.; Lee, I. J.; Lee, H.; Im, W. B. Robust Moisture and Thermally Stable Phosphor Glass Plate for Highly Unstable Sulfide Phosphors in High-Power White Light-Emitting Diodes. *Opt. Lett.* **2013**, *38*, 3298−3300.
(31) Lee, Y. K.; Lee, J. S.; Heo, J.; Im, W. B.; Chung, W. J. Phosphor in Glasses with Pb-free Silicate Glass Powders as Robust Color-Converting Materials for White LED Applications. *Opt. Lett.* **2012**, *37*, 3276−3278.
(32) Liu, P. J.; Liu, Y. L. Preparation of $CaS:Eu^{2+}$ Phosphor by Microwave Heating Method and its Luminescence. *Chin. Chem. Lett.* **2000**, *11*, 843−846.
(33) Peng, M.; Hong, G. Reduction from Eu^{3+} to Eu^{2+} in $BaAl_2O_4$:Eu Phosphor Prepared in an Oxidizing Atmosphere and Luminescent Properties of $BaAl_2O_4$:Eu. *J. Lumin.* **2007**, *127*, 735−740.
(34) Huang, L.; Wang, X.; Lin, H.; Liu, X. Luminescence Properties of Ce^{3+} and Tb^{3+} Doped Rare-Earth Borate Glasses. *J. Alloys Compd.* **2001**, *316*, 256−259.
(35) Sohn, K.-S.; Lee, S.; Xie, R.-J.; Hirosaki, N. Time-Resolved Photoluminescence Analysis of Two-Peak Emission Behavior in $Sr_2Si_5N_8:Eu^{2+}$. *Appl. Phys. Lett.* **2009**, *95*, 121903.
(36) Chen, W.-T.; Sheu, H.-S.; Liu, R.-S.; Attfield, J. P. Cation-Size-Mismatch Tuning of Photoluminescence in Oxynitride Phosphors. *J. Am. Chem. Soc.* **2012**, *134*, 8022−8025.
(37) Schmiechen, S.; Schneider, H.; Wagatha, P.; Hecht, C.; Schmidt, P. J.; Schnick, W. Toward New Phosphors for Application in Illumination-Grade White pc-LEDs: The Nitridomagnesosilicates $Ca[Mg_3SiN_4]:Ce^{3+}$, $Sr[Mg_3SiN_4]:Eu^{2+}$, and $Eu[Mg_3SiN_4]$. *Chem. Mater.* **2014**, *26*, 2712−2719.
(38) Yang, H.; Lakshminarayana, G.; Teng, Y.; Zhou, S.; Qiu, J. Tunable Luminescence from Sm^{3+}, Ce^{3+} Codoped Al_2O_3-La_2O_3-SiO_2 Glasses for White Light Emission. *J. Mater. Res.* **2009**, *24*, 1730−1734.
(39) Lin, H.; Wang, B.; Xu, J.; Zhang, R.; Chen, H.; Yu, Y.; Wang, Y. Phosphor-in-Glass for High-Powdered Remote-Type White AC-LED. *ACS Appl. Mater. Interfaces* **2014**, *6*, 21264−21269.
(40) Lin, H.; Chen, D.; Yu, Y.; Zhang, R.; Wang, Y. Molecular-Like Ag Clusters Sensitized Near-infrared Down-conversion Luminescence in Oxyfluoride Glasses for Broadband Spectral Modification. *Appl. Phys. Lett.* **2013**, *103*, 091902.
(41) Lee, G.; Im, W. B.; Kirakosyan, A.; Cheong, S. H.; Han, J. Y.; Jeon, D. Y. Tunable Emission From Blue to White Light in Single-Phase $Na_{0.34}Ca_{(0.66-x-y)}Al_{1.66}Si_{2.34}O_8:xEu^{2+},yMn^{2+}$ (x = 0.07) Phosphor for White-Light UV LEDs. *Opt. Express* **2013**, *21*, 3287−3297.
(42) Pang, R.; Li, C.; Shi, L.; Su, Q. A Novel Blue-Emitting Long-Lasting Proyphosphate Phosphor $Sr_2P_2O_7:Eu^{2+},Y^{3+}$. *J. Phys. Chem. Solids* **2009**, *70*, 303−306.
(43) Baginskiy, I.; Liu, R.-S. Significant Improvement Luminescence Intensity of Eu^{2+}-Doped $Ca_3SiO_4Cl_2$ Green Phosphor for White LEDs Synthesized Through Two-Stage Method. *J. Electrochem. Soc.* **2009**, *156*, G29−G32.
(44) Zhang, S.; Nakai, Y.; Tsuboi, T.; Huang, Y.; Seo, H. J. Luminescence and Microstructural Features of Eu-Activated $LiBaPO_4$ Phosphor. *Chem. Mater.* **2011**, *23*, 1216−1224.
(45) Tsai, C.-C.; Cheng, W.-C.; Chang, J.-K.; Chen, L.-Y.; Chen, J.-H.; Hsu, Y.-C.; Cheng, W.-H. Ultra-High Thermal-Stable Glass Phosphor Layer for Phosphor-Converted White Light-Emitting Diodes. *J. Disp. Technol.* **2013**, *9*, 427−432.
(46) Zhang, X.; Huang, L.; Pan, F.; Wu, M.; Wang, J.; Chen, Y.; Su, Q. Highly Thermally Stable Single-Component White-Emitting Silicate Glass for Organic-Resin-Free White-Light-Emitting Diodes. *ACS Appl. Mater. Interfaces* **2014**, *6*, 2709−2717.
(47) Liu, C.; Xia, Z.; Lian, Z.; Zhou, J.; Yan, Q. Structure and Luminescence Properties of Green-Emitting $NaBaScSi_2O_7:Eu^{2+}$ Phosphors for Near-UV-Pumped Light Emitting Diodes. *J. Mater. Chem. C* **2013**, *1*, 7139−7147.
(48) Liu, W.-R.; Huang, C.-H.; Wu, C.-P.; Chiu, Y.-C.; Yeh, Y.-T.; Chen, T.-M. High Efficiency and High Color Purity Blue-Emitting $NaSrBO_3:Ce^{3+}$ Phosphor for Near-UV Light-Emitting Diodes. *J. Mater. Chem.* **2011**, *21*, 6869−6874.
(49) Ding, W.; Wang, J.; Liu, Z.; Zhang, M.; Su, Q.; Tang, J. An Intense Green/Yellow Dual-Chromatic Calcium Chlorosilicate Phosphor $Ca_3SiO_4Cl_2:Eu^{2+}$-Mn^{2+} for Yellow and White LED. *J. Electrochem. Soc.* **2008**, *155*, J122−J127.
(50) Gao, G.; Wondraczek, L. Spectral Asymmetry and Deep Red Photoluminescence in Eu^{3+}-Activated $Na_3YSi_3O_9$ Glass Ceramics. *Opt. Mater. Express* **2014**, *4*, 476−485.
(51) Chen, L.-Y.; Cheng, W.-C.; Tsai, C.-C.; Chang, J.-K.; Huang, Y.-C.; Huang, J.-C.; Cheng, W.-H. Novel Broadband Glass Phosphors for High CRI WLEDs. *Opt. Express* **2014**, *22*, A671−A678.

DOI: 10.1021/acsami.5b02550
ACS Appl. Mater. Interfaces 2015, 7, 10044−10054